Turbulence Modelling for Accurate Wake Prediction in Tidal Turbine Arrays

Michael Shives* Curran Crawford†

Abstract

It is important to develop robust hydrodynamic models for predicting power output from proposed tidal turbine farms. Such models will allow for optimizing farm layout, estimating annual energy production, and predicting the temporal variation of generation. A key challenge for such models is to predict the reduction in turbine power due to wake shadowing,[1] which depends on the distance between turbines, and the wake recovery rate. Standard turbulence models over-predict the wake recovery rate, and therefore under-predict the influence of wake shadowing on power.

This paper proposes to alter standard turbulence models in two ways. The first is to limit the eddy-viscosity in close proximity to the turbine rotor to reduce the initial mixing rate. The second is to add a source of turbulent kinetic energy in the near-wake to compensate for the fact that the actuator disk approach does not resolve the discrete vortices trailed from the rotor (e.g. tip vortices), therefore under-predicting the generation of turbulence that occurrs when the vortices break-down. Comparing to two lab-scale experiments, these modifications showed significant improvement in predicting the wake recovery downstream of single turbines, and small arrays.

Keywords

tidal, turbine, actuator disc, turbulence, RANS

*Corresponding author, PhD Candidate, University of Victoria, BC, Canada, mrshives@uvic.ca

†Professor, University of Victoria, BC, Canada, curranc@uvic.ca

[1] when a turbine's wake reduces the flow entering another turbine

1 Introduction

For computational fluid dynmics (CFD) simulations of large tidal farms, it is not computationally feasible to explicitly resolve each rotor, and the influence of each rotor on the flow is often represented by adding momentum source terms to the governing equations. A common implementation of this stretegy is the actuator-disc (AD) approach (e.g. [1–3]) which applies time-averaged forces from the turbine blades over the entire rotor swept area. For turbine farm simulations the AD approach strikes a reasonable balance between accuracy and computational expense.

The AD method is well established and predicts turbine performance with high accuracy for isolated rotors [4]. However when used with standard turbulence models (k-ε or k-ω), it does not predict wake recovery accurately[5–14]. This arises due to an over estimation of the turbulent eddy viscosity in the high-shear flow within the actuator disk and near wake, which results in overly fast mixing of the wake. Additionally, the manner in which the AD averages the blade forces prevents it from resolving the discrete vortices trailed from the blades (tip vortices). The tip vortices decay into small scale turbulence as they advect downstream, but the AD approach does not capture this source of turbulent kinetic energy [15]. Despite these shortcomings, the AD is the most appropriate approach for turbine farm simulations due to its low cost and relative ease of implementation compared to fully resolving the rotor geometry or actuator line methods [16].

It is proposed herein that accurate wake simulations can be achieved by modifying standard turbulence models in two fundamental ways. The first is to limit the eddy-viscosity in close proximity to the turbine rotor to reduce the initial mixing rate, and the second is to add a source of turbulent kinetic energy in the near-wake to capture the generation of turbulence from vortex break-down.

In the context of wind turbine simulation, there have been several modifications proposed to reduce the eddy-viscosity (μ_t) in the near wake. El Kasmi and Masson [6] reduced μ_t in the k-ε model by in-

troducing a source of ε in a region surrounding the rotor. Later, Rados *et al.* [8] adapted El Kasmi and Masson's correction for use in Wilcox's k-ω model. Réthoré *et al.* [9] and Réthoré [10] tested two eddy-viscosity limiter functions for adverse pressure gradients, and *realizability* constraints; and a model adapted from forest canopy modelling. Réthoré criticized El Kasmi's model for producing an unphysical increase in ε near the rotor, which persisted downstream. Recently, Van der Laan *et al.* [14] also tested an approach which limits μ_t in regions of high strain rate, with promising results for a variety of wind farms. In the context of tidal turbines, Roc *et. al.* [12] implemented a model combining aspects of El Kasmi and Masson's correction, and Réthoré's adapted forest canopy model, showing improved agreement with porous disk experiments. Later, Shives and Crawford tested a μ_t limiter function based on the transport of Reynolds shear stress (the SST limiter of Menter [17]), showing improved agreement with scaled rotor experiments.

The concept of introducing turbulent kinetic energy into the near wake to account for vortex breakdown is relatively new, and was only recently introduced, by Shives and Crawford [15], who presented a simple modelling approach which augments the production term in the transport equation for k, improving simulation results significantly.[2] However, in that work the production augmentation terms required tuning for each case analyzed. Clearly, a generalized model is necessary for robust modelling of turbine farms, which is the focus of this paper.

The present study provides a tuning-free model for augmenting the production of k, which has been developed using data from two different experimental studies [18–20], and [21, 22] and flows with three levels of turbulence intensity (3% 10% and 15%). The resulting model was validated using a different set of experiments [21, 22], which involved two rotors in a tandem configuration, with the rotors separated by 4 to 6 diameters, and both 3% and 15% free stream turbulence intensity. The validation cases showed a very good match to the available experimental measurements of the wake recovery.

2 Validation Cases

This paper presents validation studies which compare simulation results to two different experiments. The experiments measured the turbine thrust, torque and rotational speed, as well as instantaneous velocity (u_i, i=1,2,3) along many transects downstream of the rotors. The simulations were setup to match the rotor thrust, torque and speed; while allowing the wake to develop. The quality of the simulations was assessed by comparing predictions of the mean streamwise velocity ($\overline{u}$) and turbulent kinetic energy (k) to the available data. Turbulent kinetic energy is defined as;

$$k = \frac{1}{2}\overline{u_i' u_i'} \tag{1}$$

where the tensor notation convention of summation over repeated indices is used. In this paper, k is normalized with respect to the mean freestream velocity;

$$I = \frac{\sqrt{\frac{2}{3}k}}{u_0} \tag{2}$$

where u_0 is the nominal 'freestream' velocity, typically measured at hub-height when the turbine is absent from the flow (or taken upstream of the turbine). I is referred to as the turbulence intensity and is typically expressed as a percentage.

2.1 Side-by-side rotors

The first dataset was collected by Stallard *et al.* [18–20], and involved several configurations of rotors with diameter D=27 cm. Herein, results are presented for the case with three rotors in a side-by-side arrangement (1.5D centre-to-centre spacing). The experiments were done in the University of Manchester wide flume, with a test section which is 5 m wide by 45 cm deep by 12 m long. The rotor(s) was located 6 m downstream of the test section inlet. Each rotor was coupled to a dynamometer for measuring torque, and the rotor/nacelle assembly was supported by a 15 mm diameter tower which was strain gauged for measuring thrust.

The experiments were done at 1/70 scale, bringing into question their scalability to full-size rotors. In experiments with similar turbulence intensity, Chamorro *et al.* [23] identified that rotor wake velocity profiles became Reynolds independent above $\mathrm{Re_d}\approx 4.8\times10^4$, and higher-order turbulent statistics above $\mathrm{Re_d}\approx 9.3\times10^4$. In Stallard's data-set, the Reynolds number was approximately 1.2×10^5, so the experimental results should be applicable to full-scale rotors.

Measurements of the 3 components of velocity were taken at 200 Hz using Vectrino+ acoustic doppler velocimeter (ADV) probes, allowing the calculation of

[2] Réthoré's adapted forest canopy model also introduced a source of k; but this was added at the rotor location rather than in the near wake, and was not associated with the vortex breakdown.

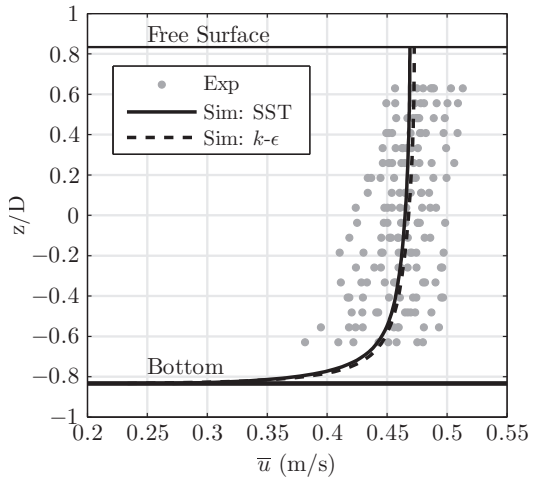

Figure 1: Vertical profile of the ambient $\overline{u}$ at the rotor location. Experimental data are shown for lateral positions spanning ±5D (±1.35 m) from the flume centreline.

Reynolds-averaged velocities and turbulence statistics. There was some variation of $\overline{u}$ with lateral position (y/D), seen as scatter in figure 1, but no discernible trend. The reference velocity u_0 was 0.47 m/s, and the depth-averaged turbulence intensity in the empty tunnel was $I \approx 10\%$ at the rotor location, decaying to ≈8% 3 m further downstream.

2.2 Tandem rotors

The second data-set was collected by Mycek *et al.* [21, 22] at the IFREMER (French Research Institute for Exploitation of the Sea) wave and current flume tank.

The rotor diameter was D=0.7 m, and the incident flow velocity was 0.8 m/s, giving a Reynolds number of 5.6×10^5, well above the threshold of 9.3×10^4 for Reynolds independent wake behaviour[23].

Both single and tandem rotor configurations were tested, using both the normal flume configuration (u_0=0.80 m/s, I=3%) and with the flow conditioning honeycombs removed (u_0=0.83 m/s, I=15%). The tunnel test section was 18 m long, 2 m wide and the water depth was 1 m. For the tandem rotor configurations, the rotors were separated axially by distances of 2D to 12D.

The model turbines were suspended into the water at mid-depth. The rotor was driven by a speed-controlled motor, with a torque cell. A load cell located above the water surface measured the total axial load acting on the rotor and its supporting structures.

The wake was measured with a traversing Laser Doppler Velocimeter, which measured the instantaneous stream-wise (u) and transverse (v) velocity components. Since the wake measurements did not include the vertical velocity components (w), it was not possible to compute k without assuming the magnitudes of $\overline{w}$ and $\overline{w'w'}$. Fortunately, when the water tunnel inflow was characterized, all three velocity components were measured, and both I_{2D} and I were reported, defined as:

$$I = \frac{\sqrt{\frac{2}{3}k}}{|\mathbf{u}|}; \qquad I_{2D} = \frac{\sqrt{\frac{1}{2}(\overline{u'u'} + \overline{v'v'})}}{|\mathbf{u}|} \tag{3}$$

Defining the ratio $\gamma = I/I_{2D}$ it is then possible to calculate k only using measured quantities:

$$k = \frac{3}{4}\gamma^2(\overline{u'u'} + \overline{v'v'}) \tag{4}$$

The value of γ was 0.87 for the 3% intensity inflow, and 1.08 for the 15% turbulence inflow. For comparing the experimentally measured k to the numerical simulations, γ was assumed constant throughout the rotor wake. Through not completely accurate, this is considered the best estimate given the available data.

3 Methodology

The simulation methodology was very similar to that presented by [15]. The simulations used the steady, incompressible, Reynolds-averaged Navier Stokes (RANS) equations, expressed below using tensor notation;

$$\frac{\partial \overline{u}_i}{\partial x_i} = 0 \tag{5}$$

$$\overline{u}_j \frac{\partial \overline{u}_i}{\partial x_j} = \frac{\partial}{\partial x_j}\left[-\frac{\overline{p}\delta_{ij}}{\rho} + 2\nu S_{ij} - \overline{u_i' u_j'}\right] + \frac{\overline{S_{Mi}}}{\rho} \tag{6}$$

where u_i is the velocity, p is the pressure, x_i is the spatial co-ordinate, ν is the fluid kinematic viscosity and ρ is the density. The overline indicates Reynolds-averaged quantities, while the prime represents fluctuating quantities. The dirac function, δ_{ij}=1 for i=j and equals zero otherwise. $\overline{S_{Mi}}$ is a Reynolds-averaged momentum-source term, used to impose the rotor forces on the flow. The term S_{ij} is the mean rate-of-strain tensor defined by:

$$S_{ij} = \frac{1}{2}\left(\frac{\partial \overline{u}_i}{\partial x_j} + \frac{\partial \overline{u}_j}{\partial x_i}\right) \tag{7}$$

3.1 The k-ω SST turbulence closure

The Reynolds stresses $\overline{u_i' u_j'}$ are determined using a turbulence closure model. The SST model is given by Menter [17]. The transport equations for turbulent

kinetic energy k and the specific dissipation rate ω are:

$$\frac{\partial \rho k \overline{u}_j}{\partial x_j} = \frac{\partial}{\partial x_j}\left[(\mu + \sigma_k \mu_t)\frac{\partial k}{\partial x_j}\right] + \tilde{P}_k - \beta' \rho k \omega + S_k \quad (8)$$

$$\frac{\partial \rho \omega \overline{u}_j}{\partial x_j} = \frac{\partial}{\partial x_j}\left[(\mu + \sigma_\omega \mu_t)\frac{\partial \omega}{\partial x_j}\right] + \alpha \frac{\rho}{\mu_t}\tilde{P}_k - \beta \rho \omega^2 + (1 - F_1)\frac{2\rho\sigma_\omega}{\omega}\frac{\partial k}{\partial x_j}\frac{\partial \omega}{\partial x_j} + S_\omega \quad (9)$$

where $P_k = \mu_t 2 S_{ij} S_{ij}$[3] is the production of k due to shear, which is limited by $\tilde{P}_k = \min(P_k, 10\beta'\rho k\omega)$ to prevent excessive production in stagnation regions. The coefficient $\beta' = 0.09$, and the other model constants (α, β, σ_k, σ_ω) are obtained by blending between constants derived for the standard k-ω model ($\alpha_1 = 5/9$, $\beta_1 = 3/40$, $\sigma_{k1} = 0.85$, $\sigma_{\omega 1} = 1/2$) and a transformed version of the k-ε model ($\alpha_2 = 0.44$, $\beta_2 = 0.0828$, $\sigma_{k2} = 1$, $\sigma_{\omega 2} = 0.856$) using the general form $\phi = \phi_1 F_1 + \phi_2(1 - F_1)$, where F_1 is a blending function given by:

$$F_1 = \tanh\left\{\left(\min\left[\max\left(\frac{\sqrt{k}}{\beta'\omega y}, \frac{500\nu}{\omega y^2}\right), \frac{4\rho\sigma_{\omega 2} k}{\mathrm{CD}_{k\omega} y^2}\right]\right)^4\right\} \quad (10)$$

$$\mathrm{CD}_{k\omega} = \max\left(\frac{2\rho\sigma_{\omega 2}}{\omega}\frac{\partial k}{\partial x_j}\frac{\partial \omega}{\partial x_j}, 10^{-10}\right) \quad (11)$$

where y is the distance to the nearest no-slip wall boundary. This function is designed such that the k-ω model coefficients are used inside the logarithmic portion of any boundary layers in the flow, whereas the k-ε coefficients are used elsewhere.

This blending approach was developed by Menter [24] to alleviate a sensitivity in the k-ω model, of the eddy viscosity to the prescribed value of ω for turbulence-free free stream conditions, by blending with the k-ε model.

As discussed by [25], two equation turbulence models tend to over predict the eddy viscosity in adverse-pressure-gradient flows where the production of k can be significantly larger than the dissipation rate. To overcome this deficiency, Menter [17] presented the following eddy viscosity formulation known as the SST limiter:

$$\mu_t = \frac{a_1 \rho k}{\max(a_1 \omega, F_2\sqrt{2 S_{ij} S_{ij}})} \quad (12)$$

which limits the eddy viscosity in regions with high turbulence production. The constant a_1 has the value 0.31, and F_2 is a second blending function:

$$F_2 = \tanh\left\{\left(\max\left[\frac{\sqrt{k}}{\beta'\omega y}, \frac{500\nu}{\omega y^2}\right]\right)^2\right\} \quad (13)$$

[3] $2 S_{ij} S_{ij} = 2\left(\frac{\partial \overline{u}}{\partial x}^2 + \frac{\partial \overline{v}}{\partial y}^2 + \frac{\partial \overline{w}}{\partial z}^2\right) + \left(\frac{\partial \overline{u}}{\partial y} + \frac{\partial \overline{v}}{\partial x}\right)^2 + \left(\frac{\partial \overline{v}}{\partial z} + \frac{\partial \overline{w}}{\partial y}\right)^2 + \left(\frac{\partial \overline{w}}{\partial x} + \frac{\partial \overline{u}}{\partial z}\right)^2$

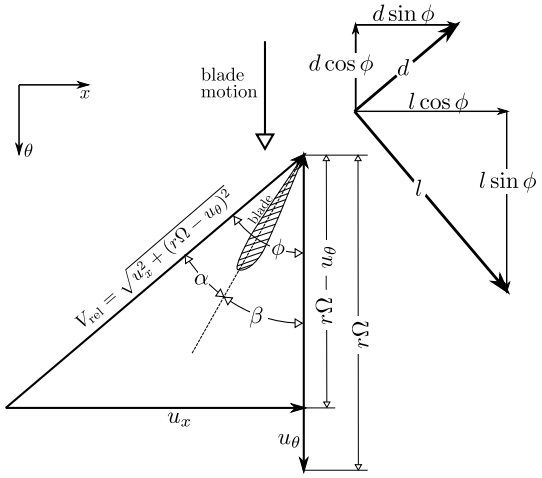

Figure 2: Flow velocities and forces acting on the blade. (u_x, u_θ)-axial and tangential velocity components, r-radial co-ordinate, Ω-rotor angular speed, β-blade twist angle, α-angle-of-attack, ϕ-inflow angle, (l, d)- lift and drag (per-unit-span)

3.2 Rotor Forces

The blade lift and drag forces were imposed using the momentum source term $\overline{S_{\mathrm{M}i}}$ in equation 6, within a sub-domain representing the swept area of the rotor. This sub-domain is referred to as the actuator disk and had the same diameter as the turbines, and a thickness of $1/10^{th}$ of the diameter. The momentum sources for each rotor were specified by using blade-element (BE) equations based-on the local flow field and tabulated lift and drag coefficients;

$$l = \frac{1}{2}\rho V_{\mathrm{rel}}^2 c \mathrm{F}_{\mathrm{tip}} c_l, \quad d = \frac{1}{2}\rho V_{\mathrm{rel}}^2 c c_d \quad (14)$$

$$\mathrm{F}_{\mathrm{tip}} = \frac{2}{\pi}\arccos\left(\exp\left(\frac{B(R - r)}{2r\sin|\phi|}\right)\right) \quad (15)$$

where V_{rel} is the flow velocity relative to the rotor blade, c is the chord length, B is the number of blades, R is the rotor radius and r is the local radial coordinate. The relative flow velocities and angles are depicted in figure 2. The term $\mathrm{F}_{\mathrm{tip}}$ is the standard Prandtl tip-loss factor (published in [26] for example). Such correction is necessary because the AD approach does not resolve the tip-vortices and thus tends to over-predict the lift near the blade tips.

The lift and drag are rotated into the rotor's cylindrical coordinate system to obtain axial and tangential force components.

$$f_x = l\cos\phi + d\sin\phi, \quad f_\theta = l\sin\phi - d\cos\phi \quad (16)$$

Time-averaging the blade force over a full revolution is done by assuming a constant rotational speed Ω, in

a manner similar to [3] to obtain the source terms:

$$\overline{S_{\mathrm{M}x}} = \frac{Bf_x}{2\pi r\Delta_x}, \quad \overline{S_{\mathrm{M}\theta}} = \frac{Bf_\theta}{2\pi r\Delta_x} \tag{17}$$

which define a force-per-unit-volume, and the term Δ_x is the finite thickness of the actuator disk.

3.2.1 Model tuning for low Re

The lift and drag coefficients must be known a priori when using the present AD method. For full-scale rotors this is usually not problematic because the variation of c_l and c_d with α and $\mathrm{Re_c}$ has been determined experimentally for a wide variety of airfoils at high Re. However, for scaled rotors, $\mathrm{Re_c}$ is often on the order $1{\times}10^5$, for which c_l and c_d are strongly dependent on $\mathrm{Re_c}$. This is problematic, because most airfoil data have been collected for higher Reynolds numbers, not covering the range typically pertaining to scaled-rotor experiments.

For the experiments by Stallard *et. al.*, which employed the Göttingen 804 airfoil, lift and drag coefficient data were available ([27]) for the Reynolds numbers used in the experiments, and the rotor forces prescribed by equations 14 to 17 gave good predictions of the rotor thrust and power. However the experiments by Mycek *et. al.* used a NACA 63-418 airfoil, for which c_l and c_d have only been published at $\mathrm{Re_c}{=}\{3,6,9\}{\times}10^6$ [28], compared to approximately $1{\times}10^5$ encountered in the experiments. At this Re, airfoil performance is sensitive to Reynolds number, turbulence intensity and surface roughness, due to the complex transition of the boundary layer from laminar to turbulent. Such behaviour is difficult to model accurately, even with very high resolution CFD simulations. Due to these sensitivities, the available airfoil coefficients were not suitable. This made it necessary to modify the momentum source terms in equation 17 to:

$$\overline{S_{\mathrm{M}x}} = A_x\frac{Bf_x}{2\pi r\Delta_x}, \quad \overline{S_{\mathrm{M}\theta}} = A_\theta\frac{Bf_\theta}{2\pi r\Delta_x} \tag{18}$$

where A_x and A_θ are coefficients which were automatically tuned as part of the CFD convergence process to match the simulation results to the experimentally measured thrust (including rotor thrust and drag acting on the structural components) and power. This approach maintained a reasonable distribution of rotor loading with radial position (via eq. 14), but ensured that the total thrust and power matched the experiments. This method isolated errors associated with the turbulence modelling from errors associated with inappropriate airfoil performance curves.

3.3 Production augmentation model for vortex-breakdown

In the AD methodology, the discrete vortices trailed from the turbine blades (particularly the tip vortices) cannot be resolved. Thus, the AD approach inherently neglects the production of k associated with the presence of trailed vortices, which are not represented in the simulations, but nonetheless do contribute to the generation of turbulent energy.

The simulations do resolve a shear layer separating the wake from the surrounding flow, and the unresolved tip vortices are spatially located within this shear layer. The resolved shear layer produces turbulent kinetic energy through the P_k term in equation 8, but this production is too small because it lacks the large shear stresses produced by the unresolved vortices. Therefore it is proposed to augment the production term P_k in the near-wake region to compensate, by adding the following source to the k equation:

$$S_k = \zeta_k P_k \tag{19}$$

In principle, S_k should be applied within a region corresponding to the break-down of the tip vortices into small-scale turbulence. A simple model is here proposed to define S_k. First, S_k is only applied within the radial limit $\{r{\leq}\sqrt{2}R\}$ (corresponding to the optimal analytical solution of the wake expanding to twice the area of the rotor). Second, the streamwise limit over which S_k is applied is defined as $\{x_0{\leq}Dx{\leq}(x_0{+}L_x)\}$, where x_0 and L_x may vary between differing test cases.

The strategy taken herein was to manually fine-tune the values of ζ_k, x_0 and L_x for a subset of the available validation cases, then determine appropriate curve-fits to define a generalized model for each parameter. This model development subset consisted of three cases; a three rotor case with 10% turbulence intensity from the data of Stallard *et. al.*, and two single-rotor cases (in 3% and 15% turbulence intensity) from the data of Mycek *et. al.*.

The distance downstream of the rotor where vortex breakdown occurs is expected to depend primarily on the streamwise velocity ($\overline{u}$), an appropriate length scale (taken here to be the diameter D), and the influence of turbulent fluctuations (defined by k and ω in the context of the SST model) in the incident flow. Using these parameters, the non-dimensional group $\frac{uD\omega}{k}$ can be composed. Considering the definition of eddy viscosity for the standard k-ω model (i.e. $\nu_t = k/\omega$) the above non dimensional group can be considered as a turbulent Reynolds number, Re_t, which uses the eddy viscosity, instead of the molecular viscosity. Thus, Re_t was considered as a suitable

predictor for the values of ζ_k, x_0 and L_x. Note that instead of using a local value of Re_t, more robust results were obtained by using the volume-averaged value of Re_t over the actuator disk sub-domain from 40% to 80% of the blade span,[4] denoted as $\mathrm{Re}_t^\star$. The determined curve-fits were as follows:

$$x_0 = \begin{cases} D\left(1400\mathrm{Re}_t^{\star\,-2} - 150\mathrm{Re}_t^{\star\,-1} + 4.5\right) & \mathrm{Re}_t^\star \geq 20 \\ 0.5D & \mathrm{Re}_t^\star < 20 \end{cases} \tag{20}$$

$$L_x = 2D \tag{21}$$

$$\zeta_k = 0.9 + 19\mathrm{Re}_t^{\star\,-1} \tag{22}$$

which were determined with $\mathrm{Re}_t^\star$ values ranging from 16 to 300.

It is possible to estimate an approximate range of Re_t in tidal channels considering analytical formulae defining a neutrally stratified logarithmic boundary layer [29]:

$$k = \frac{u^{*2}}{\beta'^{\frac{1}{2}}}, \qquad \omega = \frac{u^*}{\beta'^{\frac{1}{4}}\kappa z} \tag{23}$$

and considering the definition of turbulence intensity I (eq. 2), then the turbulent Reynolds number in a neutral log-layer can be written as:

$$Re_t = \frac{D}{\kappa\sqrt{\frac{3}{2}}Iz} \approx \frac{2D}{Iz} \tag{24}$$

where $\kappa = 0.41$ is the von Karman constant and z is the hub height above the seabed. Given a turbine with diameter 20 m at a hub height of 30 m, and a flow with 10% intensity, Re_t would be roughly 13, which is below the range employed in the present study. It may be that an alternate predictor variable will need to be chosen to scale the model to full size rotors, or future experiments may need to be run to expand the range of tested Re_t.

Note that in the present implementation, for tandem rotor configurations, the production augmentation zone of an upstream rotor is limited to the region upstream of the next rotor.

3.4 Boundary Conditions and Mesh

The simulation domain was the entire tunnel test section. Constant values for $\overline{u}$, k and ε were set at the inlet, which were tuned to match the experimental 'inflow' velocity and turbulence intensity, which, for both experimental campaigns, were measured slightly upstream of the model turbines. The resulting profile for Stallard's experiment is shown in figure 1. The structural components of the turbine models were resolved by the mesh. The tunnel walls and surfaces of the structural components used a smooth-wall no-slip condition and employed the 'automatic' wall treatment provided by CFX [30], which uses wall functions to compute the wall shear stress and an analytical solution to set the value of ω. A typical pressure outlet condition was used. The water free-surface was modelled as a rigid lid (no surface deformation) using a free-slip wall.

The mesh was generated using a similar topology and spacings (relative to the rotor diameter) as the 'mesh B' from [15], which was shown to provide grid independent solutions of both turbine performance and wake recovery. The mesh used 4 elements spanning the actuator disk thickness, 48 elements across its diameter, and 72 elements azimuthally (5° segments). The element sizes were not uniform, and the mesh was refined to provide good resolution of the boundary layer on the hub and tower, and of the strong shear layer at the edge of the actuator disk.

4 Wake Validation

The velocity and turbulence levels in the rotor wakes are compared to experimental data in this section. Results are first presented for the case of three rotors in a side-by-side configuration, and then for the tandem rotor cases.

4.1 Results for side-by-side rotors

Figures 3, and 4 show the streamwise velocity and turbulence intensity in the wake for the three-rotor side-by-side configuration. The simulations using the standard k-ε turbulence model are shown as a baseline. As reported by many previous studies, the standard k-ε model predicts much faster wake recovery than the experimental data. It also fails to predict the distinct peeks in the turbulence intensity located at the edges of the wake. The SST turbulence model improves the prediction of the wake velocity profiles, but somewhat overcompensates, resulting in slightly too slow wake recovery. The SST model predicts a better spatial pattern of turbulence intensity in the wake, but the intensity is too low. Incorporating the S_k term to account for the generation of k by the unresolved tip vortices improves the prediction of turbulence intensity in the wake, and gives good predictions of the wake velocity profiles. For this case, the turbulent Reynolds number was $\mathrm{Re}_t^\star$=37, giving x_0=1.45D, ζ_k=1.4 (similar values for all 3 rotors).

[4] Using the region from 40% to 80% span makes the approach more robust by eliminating sensitivities to grid resolution in the nacelle boundary layer and strong shear layer at the blade tip.

Good results were expected for this case because it was used for developing the curve-fits for x_0 and ζ_k.

4.2 Results for Tandem Rotor Cases

Figures 5 to 6 show results for low ambient turbulence (3%) for the tandem rotor cases from the experiments, with the rotors separated by 4D and 6D. Results from the standard k-ω model are shown as a baseline. As, expected, the standard k-ω model significantly over predicts the wake recovery rate. The SST model improves the prediction of the wake recovery, showing very good results for the case with 4D separation between rotors (figure 5), but slightly worse predictions for 6D (figure 6). Using the S_k model improved the predictions of k in the wake for both 4D and 6D separation distances. The match to experimental data is very good for the 6D case, while for the 4D case it is apparent that S_k could have been applied closer to the rotor to achieve better results. These cases validate the S_k model for the scenario of a rotor directly in the wake of an upstream rotor.

Figures 7 and 8 show results for high ambient turbulence (15%) for two-rotor arrays, with the rotors separated by 4D and 6D, respectively. For this high turbulence scenario, the baseline k-ω model over predicts the wake recovery, but not as severely as for the low turbulence cases. The k-ω model also misrepresents the shape of the wake, predicting a very narrow wake, and grossly under predicts the turbulence intensity. The SST model improves the wake shape somewhat, but under predicts the velocity recovery and the turbulence intensity. Including the S_k model improves the prediction of turbulence intensity. It also improves the velocity predictions downstream of 3D, but causes the wake to recover too much between 1D and 2D. Overall, the SST+S_k model gives the best match to the experiments.

Note that for the high turbulence cases, the flow was less controlled because the flow conditioning honeycombs were removed from the tunnel. This likely explains the asymmetry in the velocity and turbulence profiles. It may also explain why the turbulence decays faster in the simulations than in the tunnel, since it is likely that the tunnel flow contained flow features (i.e. secondary flows) which produced turbulence through shear. In any case, it was naturally more difficult to achieve a good match between experiment and simulation for the high turbulence cases.

5 Discussion & Future Work

This paper has presented a novel turbulence modelling approach for use with actuator disk simulations of tidal (or wind) turbines. It is a well known problem that standard RANS turbulence models do not provide good predictions of turbine wakes. Accurate wake prediction is vital for simulations of turbine farms, where wake interactions can alter turbine performance significantly. There have been several studies investigating modifications to improve wake predictions by altering the eddy viscosity. This paper found that the SST eddy viscosity limiter is suitable for this purpose.

In addition, this paper argues that the AD method inherently neglects the discrete vortices trailed from the blades (particularly the tip vortices), instead resolving a shear layer at the edge of the wake. The turbulence production resolved by AD simulations therefore only contains a component due to shear in the Reynolds averaged flow, but lacks production arising from the strong shear layers caused by the tip vortices, and also lacks the generation of turbulence from vortex breakdown. Thus, it is proposed to augment the turbulence production term in the turbine near-wake. This paper presents a simple model to prescribe such augmentation, which has been tuned through comparison to experimental data. The model was found to provide very good predictions of the velocity and turbulence intensity in turbine wakes from scaled rotor experiments. The validation data-set (which was not used for tuning the model) included scenarios with two rotors in a tandem configuration, separated by 4D and 6D, and in flows with ambient turbulence intensities of 3% and 15%.

Thus far, the proposed approach, which involves the SST turbulence model, combined with the turbulence production augmentation model, has been validated using lab-scale experimental data. The choice to use lab-scale data was taken because of the greater spatial density of data, lower uncertainty, and better flow characterization possible compared to full-scale field data. Presently, the authors are not aware of any field-scale tidal turbine data-sets which could be used to validate the model, however there are several suitable studies from wind farms. Future testing with field data will be necessary to fully validate the method. More work is needed to asses the applicability of the proposed approach in the context of full-scale ABL flows and tidal channel boundary layers. Finally, the presented simulations in this study explicitly resolved the structural components of the turbine models (i.e. the hub and tower) which some-

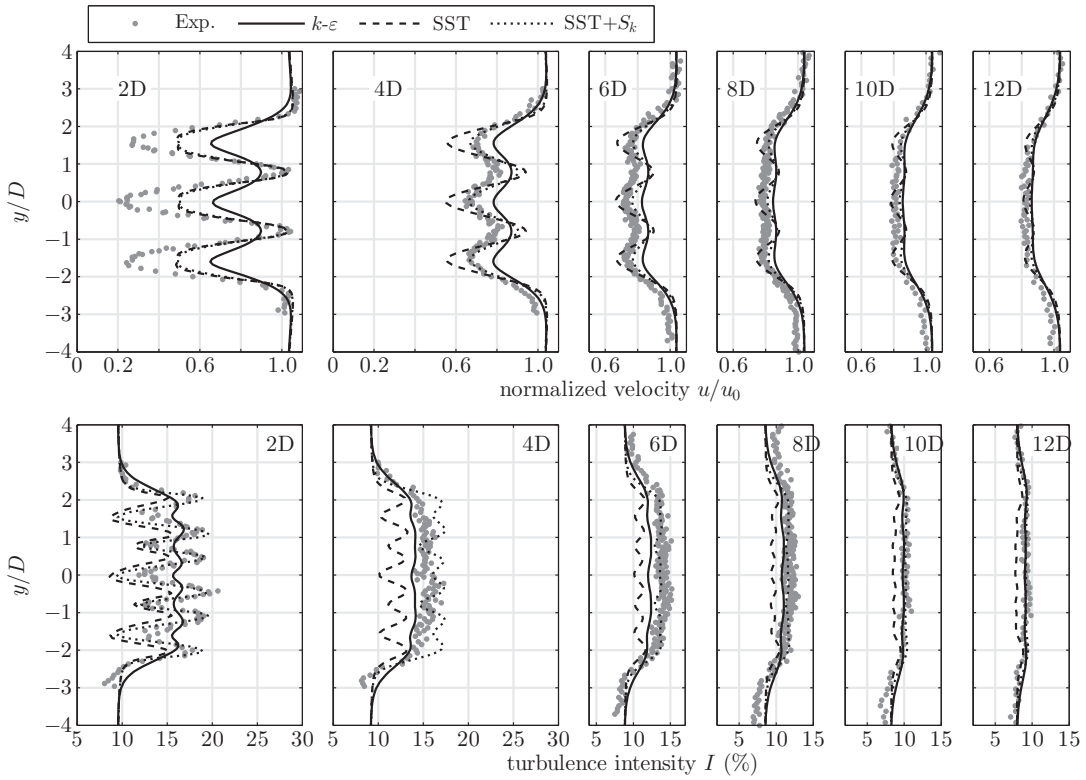

Figure 3: Lateral profiles of velocity and turbulence intensity for the three wakes downstream of the rotors in the experiments by Stallard *et al.*

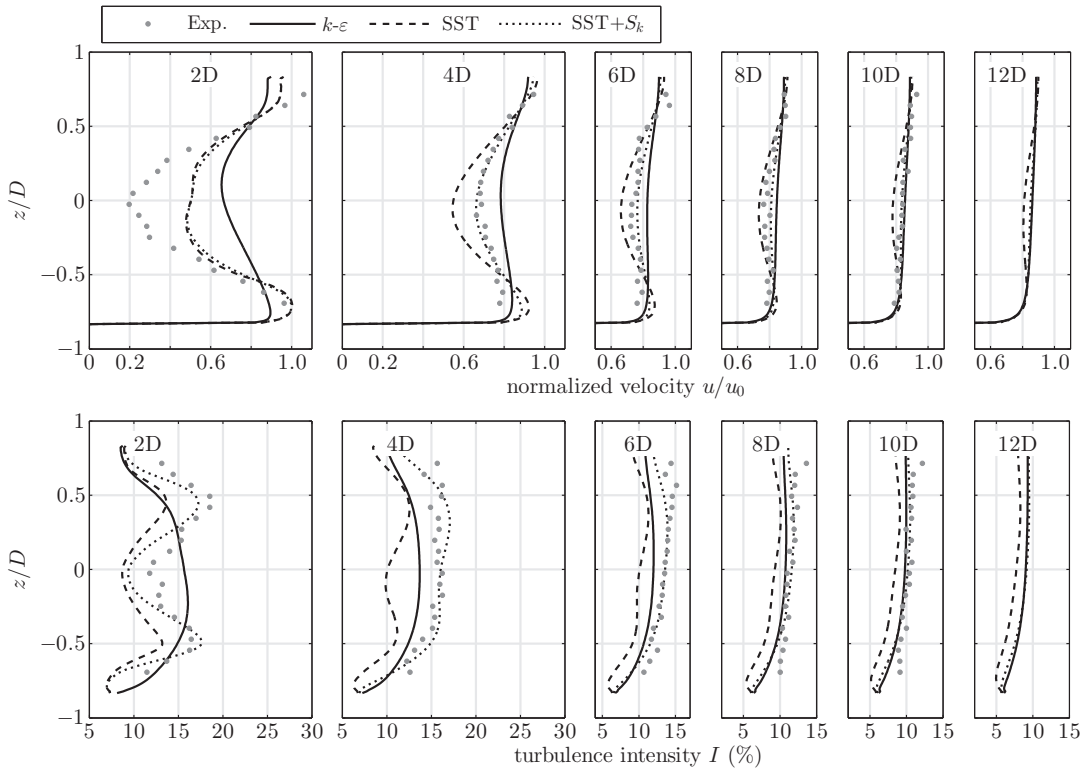

Figure 4: Depthwise profiles of velocity and turbulence intensity for the wake downstream of the central rotor in the experiments by Stallard *et al.*

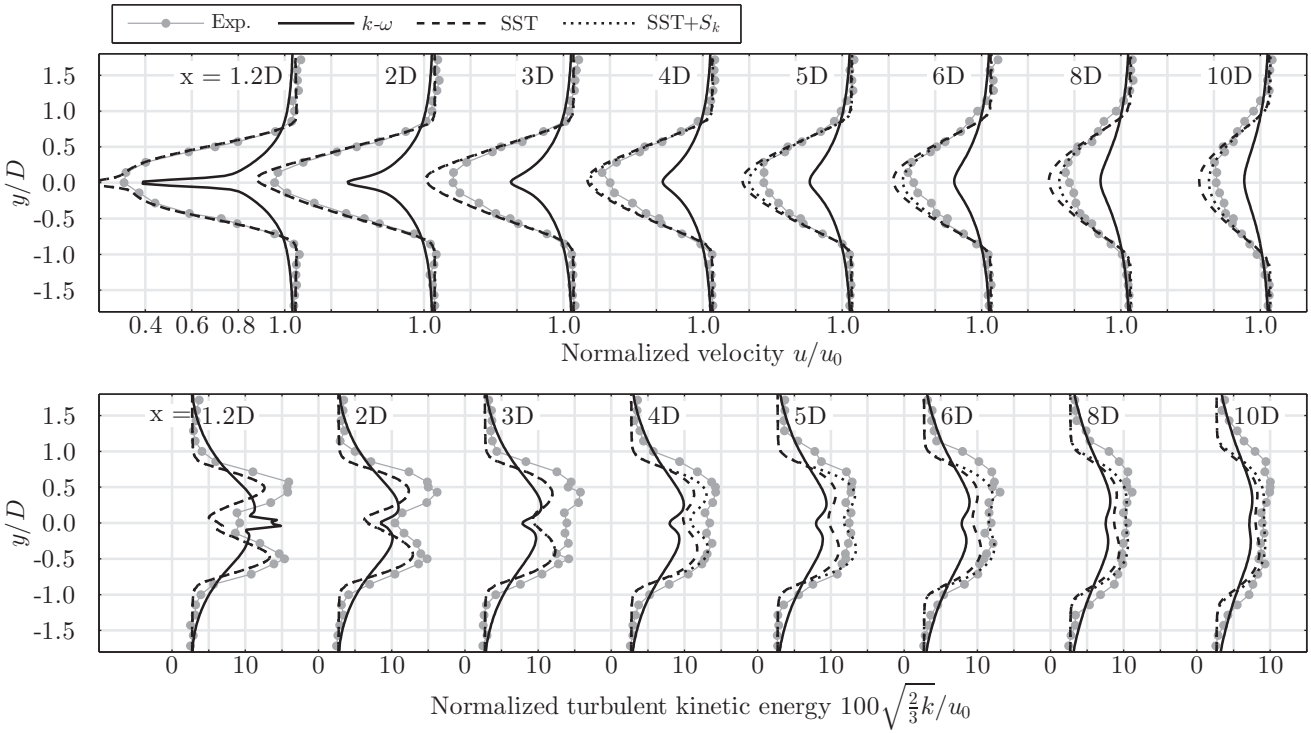

Figure 5: Profiles of normalized u and k for 3% inflow intensity. Profiles are downstream of the second rotor in a twin rotor configuration with stream-wise separation of 4D.

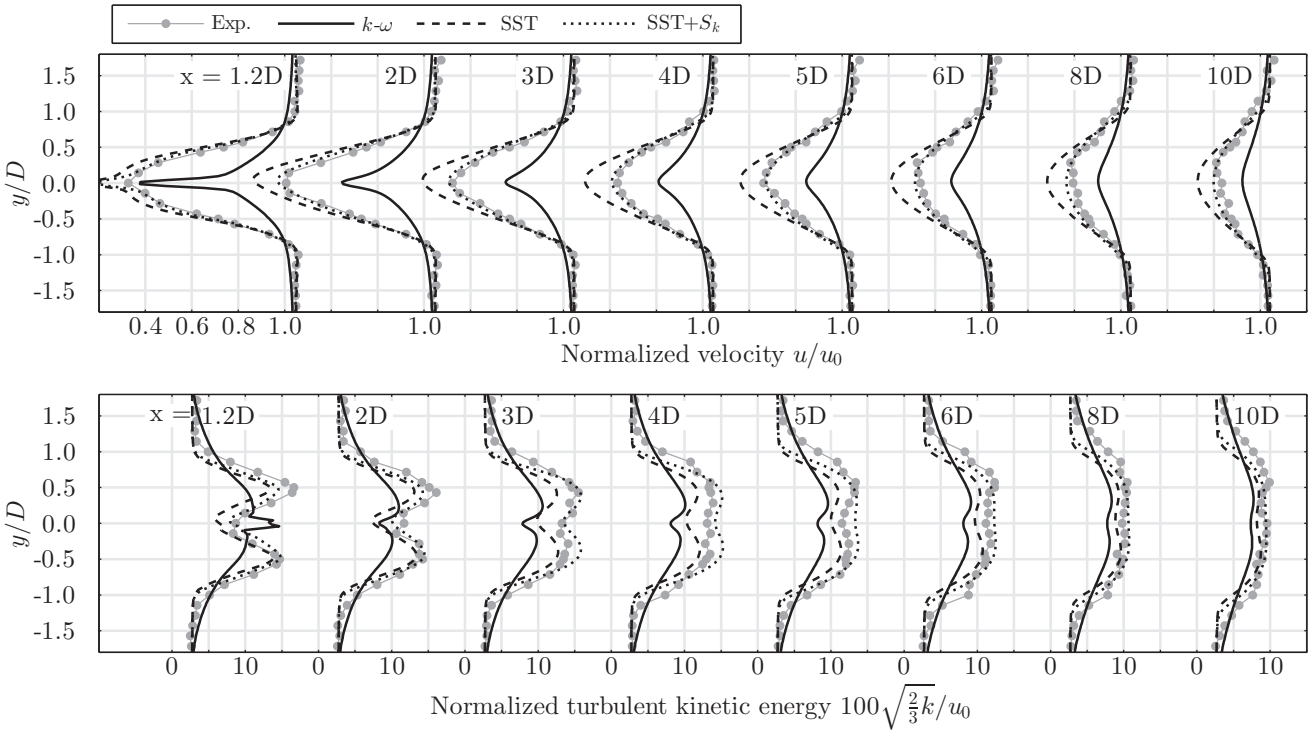

Figure 6: As figure 5, but with stream-wise separation of 6D between rotors. (I=3%)

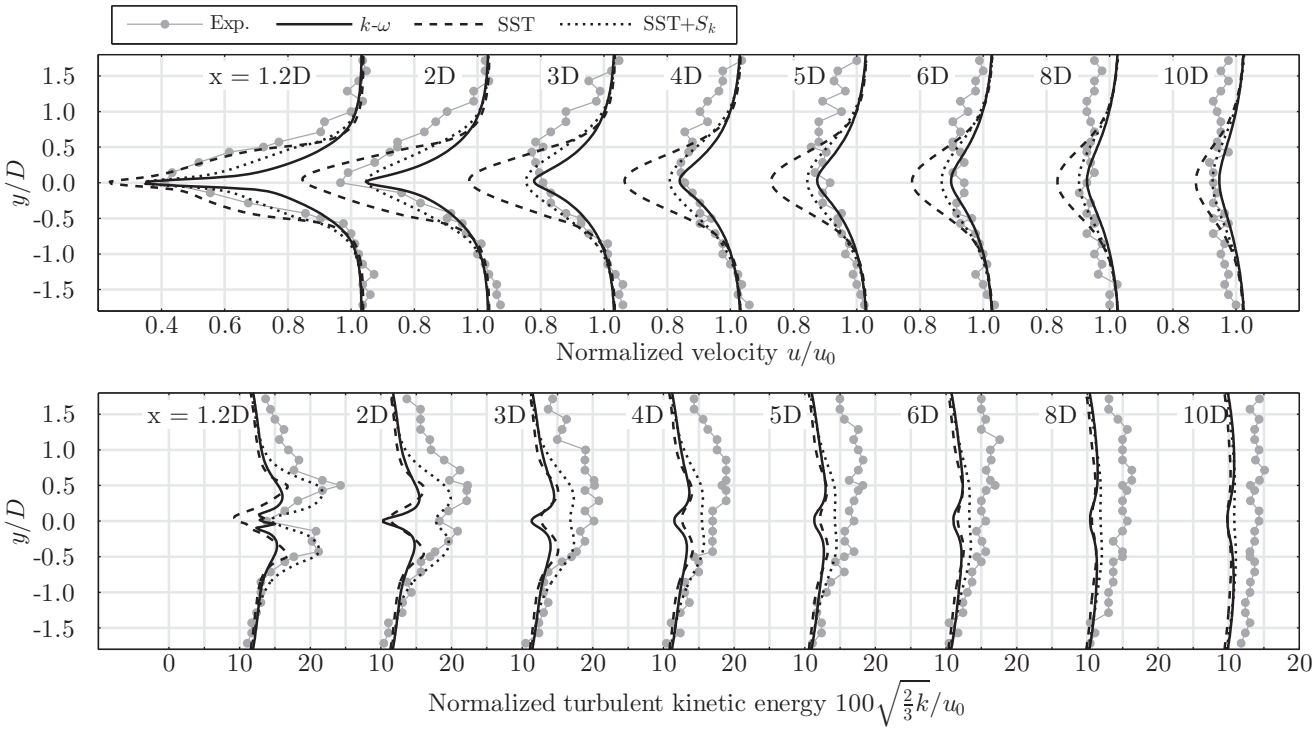

Figure 7: Profiles of normalized u and k for 15% inflow intensity. Profiles are downstream of the second rotor in a twin rotor configuration with stream-wise separation of 4D.

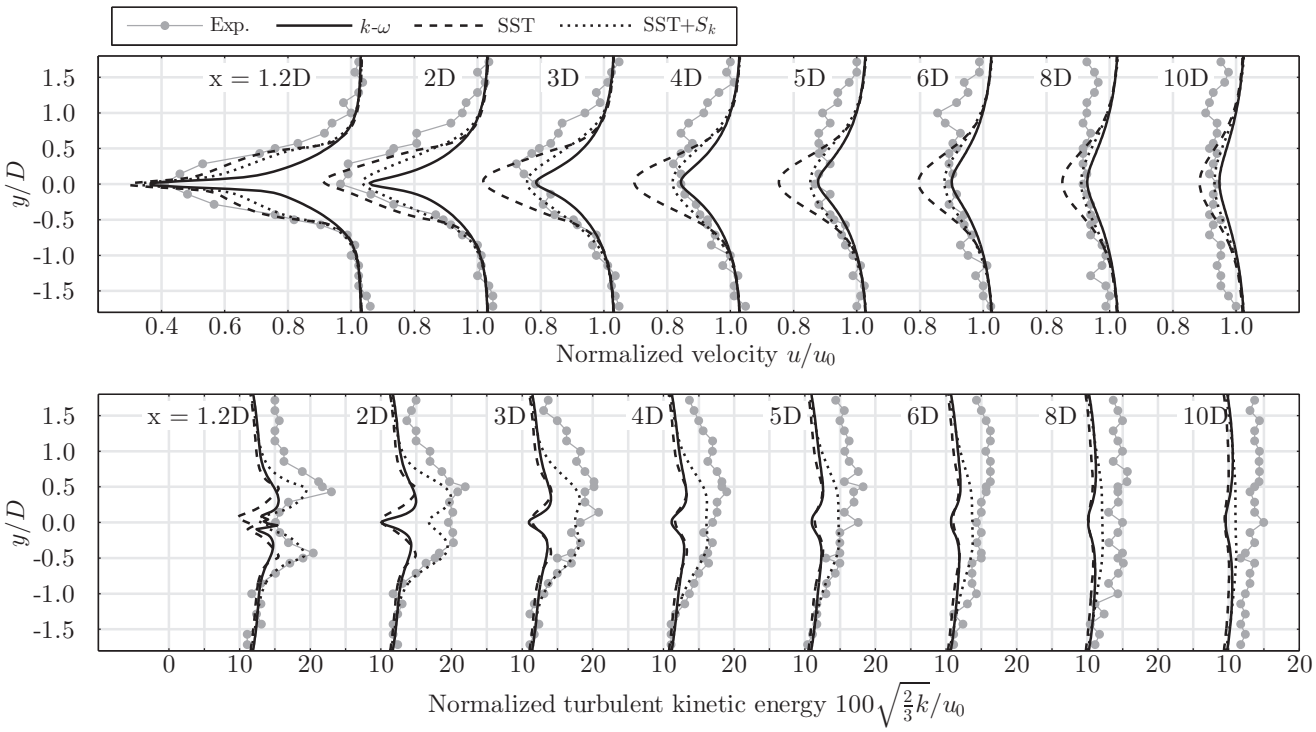

Figure 8: As figure 7, but with stream-wise separation of 6D between rotors.

what undermined the value of using the AD approach, since its purpose is to allow coarse mesh resolution and fast simulations. Thus, future work will also focus on developing methods to represent the structural components with coarser meshes.

Acknowledgments

The authors thank the National Sciences and Engineering Research Council (NSERC) of Canada and the University of Victoria for financial support.

References

[1] Mikkelsen, R. *Actuator Disc Methods Applied to Wind Turbines*. PhD, University of Denmark, 2003 1

[2] Castellani, F. and Vignaroli, A. "An application of the actuator disc model for wind turbine wakes calculations." *Applied Energy*, (p. 432440), 2013

[3] Ammara, I., Leclerc, C., and Masson, C. "A Viscous Three-Dimensional Differential/Actuator-Disk Method for the Aerodynamic Analysis of Wind Farms." *Journal of Solar Energy Engineering*, 124: pp. 343–356, 2002 1, 5

[4] Réthoré, P.-E., van der Laan, P., Troldborg, N., Zahle, F., and Sørensen, N. N. "Verification and validation of an actuator disc model." *Wind Energy*, Published online in Wiley Online Library (wileyonlinelibrary.com). DOI: 10.1002/we.1607, 2013 1

[5] Crespo, A., Manuel, F., Moreno, D., Fraga, E., and Hernandez, J. "Numerical analysis of wind turbine wakes." In "Proceedings of Delphi Workshop on Wind Energy Applications, Delphi, Greece, pp. 15-25," 1985 1

[6] El Kasmi, A. and Masson, C. "An extended k-ϵ model for turbulent flow through horizontal-axis wind turbines." *Journal of Wind Engineering and Industrial Aerodynamics*, 96: pp. 103–122, 2008 1

[7] Cabezón, D., Sanz, J., Marti, I., and Crespo, A. "CFD modelling of the interaction between the Surface Boundary Layer and rotor wake: Comparison of results obtained with different turbulence models and mesh strategies." In "Proceedings of the European Wind Energy Conference," 2009

[8] Rados, K., Prospathopoulos, J., Stefanatos, N., Politis, E., Chaviaropoulos, P., and Zervos, A. "CFD modeling issues of wind turbine wakes under stable atmospheric conditions." In "European Wind Energy Conference, Marseille," 2009 2

[9] Réthoré, P. E., Sørensen, N. N., Bechmann, A., and Zhale, F. "Study of the atmospheric wake turbulence of a CFD actuator disc model." In "European Wind Energy Conference, Marseille," 2009 2

[10] Réthoré, P. E. *Wind Turbine Wake in Atmospheric Turbulence*. PhD, Aalborg University, 2009 2

[11] Prospathopoulos, J. M., Politis, E. S., Rados, K. G., and Chaviaropoulos, P. K. "Evaluation of the effects of turbulence model enhancements on wind turbine wake predictions." *Wind Energy*, 14: pp. 285–300, 2011

[12] Roc, T., Conley, D. C., and Greaves, D. "Methodology for tidal turbine representation in ocean circulation model." *Renewable Energy*, 51: pp. 448–464, 2013 2

[13] AbdelSalam, A. M. and Ramalingam, V. "Wake prediction of horizontal-axis wind turbine using full-rotor modeling." *Journal of Wind Engineering and Industrial Aerodynamics*, 124: pp. 7–19, 2014

[14] van der Laan, M. P., Sørensen, N. N., Réthoré, P.-E., Mann, J., Kelly, M. C., Troldborg, N., Schepers, J. G., and Machefaux, E. "An improved k-ϵ model applied to a wind turbine wake in atmospheric turbulence." *Wind Energy*, Published online in Wiley Online Library, 2014. doi: 10.1002/we.1736 1, 2

[15] Shives, M. and Crawford, C. "Adapted two-equation turbulence closures for actuator disk RANS simulations of wind & tidal turbine wakes." *Renewable Energy*, 2014. Under Review 1, 2, 3, 6

[16] Sørensen, J. N. and Shen, W. Z. "Numerical Modeling of Wind Turbine Wakes." *Journal of Fluids Engineering*, 124: pp. 393–399, 2002 1

[17] Menter, F. R. "Review of the shear-stress transport turbulence model experience from an industrial perspective." *International Journal of Computational Fluid Dynamics*, 23(4): pp. 305–316, 2009 2, 3, 4

[18] Whelan, J. I. and Stallard, T. "Arguments for modifying the geometry of a scale model rotor." In "European Wave and Tidal Energy Conference Series," 2011 2

[19] Stallard, T., Collings, R., Feng, T., and Whelan, J. "Interactions Between Tidal Turbine Wakes: Experimental Study of a Group of 3-Bladed Rotors." In "European Wave and Tidal Energy Conference Series," 2011

[20] Stallard, T., Collings, R., Feng, T., and Whelan, J. "Interactions between tidal turbine wakes: experimental study of a group of three-bladed rotors." *Phil Trans R Soc A*, 371: pp. 1–13, 2013. doi:20120159 2

[21] Mycek, P., Gaurier, B., Germain, G., Pinon, G., and Rivoalen, E. "Experimental study of the turbulence intensity effects on marine current turbines behaviour. Part I: One single turbine." *Renewable Energy*, 66: pp. 729–746, 2014 2, 3

[22] Mycek, P., Gaurier, B., Germain, G., Pinon, G., and Rivoalen, E. "Experimental study of the turbulence intensity effects on marine current turbines behaviour. Part II: Two interacting turbines." *Renewable Energy*, 68: pp. 876–892, 2014 2, 3

[23] Chamorro, L. P., Arndt, R. E. A., and Sotiropoulos, F. "Reynolds number dependence of turbulence statistics in the wake of wind turbines." *Wind Energy*, 15: pp. 733–742, 2012 2, 3

[24] Menter, F. "Influence of Freestream Values on k-ω Turbulence Model Predictions." *AIAA Journal*, 30: pp. 1651–1659, 1992 4

[25] Menter, F. R. "Two-Equation Eddy-Viscosity Turbulence Models for Engineering Applications." *AIAA Journal*, 32: pp. 1598–1605, 1994 4

[26] Burton, T., Sharpe, D., Jenkins, N., and Bossanyi, E. *Wind Energy Handbook*. John Wiley & Sons Ltd., 2001 4

[27] Hassan, U. "A wind tunnel investigation of the wake structure within small wind turbine farms." Report no ETSU WN 5113, 1993 5

[28] Abbott, I. H., von Doenhoff, A. E., and Stivers Jr, L. S. "Summary of Airfoil Data." Report No 824, NACA, 1945 5

[29] Panofsky, H. and Dutton, J. *Atmospheric Turbulence*. Wiley, New York, 1984 6

[30] ANSYS, I. "ANSYS CFX-Solver Theory Guide." ANSYS, Inc., 275 Technology Drive, Canonsburg, PA 15317, 2013. Http://www.ansys.com 6